J. Membrane Biol. 91, 213–225 (1986)

The Journal of
Membrane Biology

Membrane Transport Parameters in Frog Corneal Epithelium Measured Using Impedance Analysis Techniques

Chris Clausen,† Peter S. Reinach‡ and Daniel C. Marcus§

† Department of Physiology and Biophysics, Health Sciences Center, State University of New York at Stony Brook, Stony Brook, New York 11794-8661, ‡ Departments of Ophthalmology and Physiology and Cell Biology, and § Department of Otolaryngology, Washington University School of Medicine, St. Louis, Missouri 63110

Summary. Active Cl^- transport in bullfrog corneal epithelium was studied using transepithelial impendance analysis methods, and direct-current (DC) measurements of membrane voltages and resistance ratios. The technique allows the estimation of the apical and basolateral membrane conductances, and the paracellular conductance, and does not rely on the use of membrane conductance-altering agents to obtain these measurements as was requisite in earlier DC equivalent-circuit analysis studies. In addition, the analysis results in estimates of the apical and basolateral membrane capacitances, and allows resolution of the paracellular conductance into properties of the tight junctions and lateral spaces. Membrane capacitances (proportional to areas) were used to estimate the specific conductances of the apical and basolateral membranes, as well as to evaluate coupling between the cell layers. We confirm results obtained from earlier studies: (1) apical membrane conductance is proportional to the rate of active Cl^- transport and is highly Cl^- selective; (2) intracellular Cl^- activity is above electrochemical equilibrium, thereby providing a net driving force for apical membrane Cl^- exit; (3) the paracellular conductance is comparable to the transcellular conductance. We also found that: (1) the paracellular conductance is composed of the series combination of the junctional conductance and a nonnegligible lateral space resistance; (2) a small K^+ conductance reported in the apical membrane may result from Cl^- channels possessing a finite permeability to K^+; (3) the basolateral membrane areas is 36 times greater than the apical membrane area which is consistent with the notion of electrical coupling between the five to six cell layers of the epithelium; (4) the specific conductance of the basolateral membrane is many times lower than that of the apical membrane; (5) the net transport of Cl^- is modulated primarily by changes in the conductance of the apical membrane and not by changes in the net electrochemical gradient resulting from opposite changes in the electrical and chemical gradients; (6) the conductance of the basolateral membrane does not change with transport which implies that the net driving force for K^+ exit increases with transport, possibly due to an increase in the intracellular K^+ activity.

Key Words corneal epithelium · corneal endothelium · Cl^- transport · impedance analysis · equivalent circuit analysis · cell coupling

Introduction

Active Cl^- transport across the isolated frog corneal epithelium includes coupled NaCl uptake across the basolateral membrane from the stromal bathing solution, followed by Cl^- electrodiffusion across the Cl^- permselective apical membrane into the tear-side bathing solution. Direct-current (DC) equivalent circuit analysis techniques have been used in conjunction with the measurement of intracellular ion activities to determine the cellular membrane ionic conductances and the conductance of the paracellular pathway comprising the tight junctions and the lateral spaces (Nagel & Reinach, 1980; Patarca et al., 1983; Reuss et al., 1983; Reinach & Nagel, 1985). However, investigators were faced with the problem of separating measurements of the transepithelial conductance into the conductances of the transcellular and paracellular pathways.

The DC equivalent circuit techniques require the use of an agent which changes the rate of active ion transport by selectively altering a single membrane (e.g., apical) conductance (Reuss & Finn, 1974). When the time-dependent effects of the agent on the transepithelial conductance and short-circuit current are plotted against one another, the paracellular conductance is determined from the zero-current intercept of the resulting linear relationship between these parameters. The transcellular conductance is the difference between the transepithelial and paracellular conductances, and can subsequently be resolved into properties of the apical and basolateral membranes using microelectrode resistance-ratio measurements. The success of this approach also requires that the conductance-altering agent acts rapidly, and that it is reversible.

A number of different agents were used for this purpose in these studies of the cornea. It was assumed that epinephrine and adenosine stimulate active Cl^- transport by increasing apical membrane Cl^- conductance, and the loop diuretics (e.g., furosemide and bumetanide) inhibit transport by decreasing apical membrane Cl^- conductance. However, these agents may not act selectively on the apical membrane. Epinephrine and the loop diuret-

ics are known to alter basolateral membrane properties in the cornea and other tissues (Nagel & Reinach, 1980; Welsh et al., 1983; Greger & Schlatter, 1983, 1984; Smith & Frizzel, 1984), and the selective action of adenosine has not been verified (Reuss et al., 1983). Therefore, there exists some doubt whether or not these agents are appropriate for determining reliable estimates of the cellular membrane and paracellular conductances.

DC equivalent circuit analysis methods may suffer from other possible problems, and are also incapable of addressing other questions regarding the mechanism of active Cl^- transport in the cornea. First, when measuring membrane resistance ratios with microelectrodes, one generally ignores the lateral-space resistance which is in series with the basolateral membrane. The lateral spaces are seen to be narrow (*ca.* 10 nm) and follow a long tortuous path (>50 μm) from the tight junctions to the stroma, and therefore may constitute a resistance comparable to that of the basolateral membrane. Hence, these microelectrode measurements may result in underestimates of the true cellular membrane resistance ratios. Second, DC circuit analysis methods cannot resolve the paracellular conductance into properties of the tight junctions and lateral spaces. And third, the corneal epithelium consists of five to six cell layers which appear to be coupled electrically (Klyce, 1972). The relationships between the apical and basolateral membrane conductances and their respective specific conductances (conductances per unit area of membrane) are not known since these estimates require knowledge of the membrane areas which are dependent on the degree of coupling between the cell layers.

The purpose of this study was to use impedance analysis techniques, in conjunction with DC microelectrode measurements of membrane resistance ratios, to investigate how the rate of Cl^- secretion is regulated by changes in the apical, basolateral, and paracellular conductances, in the isolated frog corneal epithelium. The impedance techniques do not rely on the use of membrane conductance-altering agents in order to separate transepithelial and microelectrode measurements into properties of each of the different membranes; epinephrine and furosemide were used merely to vary Cl^- secretion rate. In many cases, impedance techniques are capable of determining the lateral-space conductance, which allows one to correct measurements of the apparent resistance ratios for this added series resistance, and also permits resolution of the paracellular conductance into properties of the tight junctions and the lateral spaces. Finally, impedance analysis techniques also result in estimates of the apical and basolateral membrane capacitances. Since membrane capacitance is directly proportional to actual membrane area, possessing a proportionality constant of approximately 1 $\mu F/cm^2$ (Cole, 1972), these values allow one to normalize the different membrane conductances to unit area of membrane thereby yielding estimates of the membranes' specific conductances. Estimates of basolateral membrane capacitance also allow one to evaluate cell coupling between the different cell layers.

Materials and Methods

Animals and Chamber Design

Bullfrogs (*Rana catesbeiana*) were double pithed, and their corneas were excised and mounted in a modified Ussing chamber that was specifically designed to eliminate edge damage (for details on the chamber design, consult Lewis et al., 1977). The preparation was mounted vertically, sealed with silicone vacuum grease, and supported by a nylon mesh on the stromal side. Nominal tissue area was 0.28 cm^2. Each half-chamber had a volume of 15 ml, and was continually stirred using small magnetic fleas. All experiments were carried out at room temperature.

Solutions

The tissue was bathed symmetrically with solutions of the following composition (in mM): NaCl 109.2, KCl 2.5, $CaCl_2$ 1.0, and dextrose 10.0. The solutions were buffered to pH 8.1 using 1 mM HEPES. Active Cl^- transport was increased by the addition of 0.1 mM epinephrine (Sigma Chemical, St. Louis, Mo.) to the stromal side, and was inhibited by washing the stromal solution and (in some cases) by the subsequent addition of 1 mM furosemide (Hoechst-Roussel Pharmaceuticals, Somerville, N.J.).

Transepithelial Electrical Measurements

Transepithelial voltage was measured differentially using a pair of Ag-AgCl electrodes mounted immediately adjacent to the preparation, and connected to a low-noise high-impedance amplifer (model 113, Princeton Applied Research, Princeton, N.J.). The voltage was continuously recorded on a chart recorder (Houston Ins., Austin, Tex.). A second set of Ag-AgCl electrodes mounted at opposite ends of the chamber was used to pass transepithelial current. The stromal current electrode was grounded, and constant current was generated using a calibrated 1 or 10 MΩ carbon series resistor. The rate of active Cl transport under short-circuit conditions was represented as the short-circuit current (I_{sc}) (Zadunaisky, 1966), and was measured intermittently by passing a 500-msec current pulse which zeroed the transepithelial voltage (no correction was made for the small, *ca.* 100 Ωcm^2, series resistance of the solution between the voltage electrodes and the preparation). The voltage drop across the 1 or 10 MΩ series resistor is proportional to I_{sc}, and was measured using a three-digit voltmeter.

The Ag-AgCl electrodes were constructed by dipping polished silver wires into molten AgCl, as opposed to the more traditional electroplating technique. This produced electrodes with lower capacitance, lower asymmetry potentials, and better current-passing capability.

Intracellular Microelectrode Techniques

Conventional microelectrodes were pulled on a horizontal puller (model PD-2, Narishige, Japan) from 1.2 mm borosilicate glass [either fiber-filled (W-P Instruments, New Haven, Conn.) or delta glass (A-M Systems, Everett, Wash.)]. They were filled with filtered 3 M KCl, and had resistances between 15 and 40 MΩ. They were connected by means of a Ag-AgCl electrode holder to one channel of a differential high-impedance electrometer (W-P Instruments, New Haven, Conn.); the other channel of the electrometer was connected directly to the stromal electrode. Voltage measurements were recorded continuously on a chart recorder (Gould, Cleveland, Ohio).

Impalements were made by passing the microelectrode down through an open port in the front chamber, and penetrating the tissue from the apical side at a 45-degree angle. Since the electrode was referenced to the stromal side, prior to penetration it measured the transepithelial voltage, and after penetration it measured the basolateral membrane voltage. Positioning was performed using a remote-controlled micromanipulator (model STM3, Stoelting, Germany). Visual placement of the electrode was aided by a horizontally mounted dissecting microscope. The chamber and micromanipulator were mounted on a flotation table (Newport Research, Fountain Valley, Calif.) to minimize outside vibrations. Microelectrode penetrations were considered acceptable if they satisified three criteria: (1) an abrupt change in voltage as the electrode initially entered a cell; (2) a stable potential with negligible drift for the duration of the penetration (typically 20 sec); and (3) an abrupt return of the electrode voltage to the same value prior to the penetration after the electrode was retracted.

Apparent apical-to-basolateral membrane resistance ratios were obtained by measuring the transepithelial and basolateral voltage deflections (ΔV_t and ΔV_b, respectively) resulting from 500-msec depolarizing transepithelial current pulses. The amplitudes of the pulses were adjusted to produce a ΔV_t of approximately 20 mV. The voltage deflections were read off the chart recorder with an accuracy of better than 0.3 mV. The resistance ratio was calculated as $\alpha = \Delta V_t/\Delta V_b - 1$. Typically six measurements, each from different regions of the preparation, were taken for each impedance run (three immediately before and after), and the resulting mean value of α was used for equivalent-circuit calculations. In all cases, our measurements were in good agreement with those previously reported when measured under the same experimental conditions (Nagel & Reinach, 1980; Patarca et al., 1983; Reuss et al., 1983).

Measurement of Transepithelial Impedance

Transepithelial impedance was measured over the range of 2 Hz to 9.1 kHz using the method of Clausen and Fernandez (1981). A wide-band (pseudo-random binary) constant current signal (10 $\mu A/cm^2$ peak-to-peak) was generated using a digital shift-register circuit. Prior to an experiment, the current was recorded and characterized by measuring the voltage response to the current in the empty chamber filled only with NaCl Ringer's solution, or by measuring the voltage response across a calibrated 1 kΩ carbon resistor (one experiment). Subsequently, the transepithelial impedance was calculated as the Fourier transform of the epithelial voltage response to the current, divided by the Fourier transform of the current. The impedance of the empty chamber and electrodes was verified to be totally resistive; the resulting phase angle was less than 0.5 degrees over the frequency range. This is expected since phase deviations arising from our major stray capacitance, the input capacitance of the amplifier (15 pF), are negligible due to the low resistance of the Ag-AgCl electrodes (*ca.* 1 kΩ).

During the impedance runs, the transepithelial differential amplifier was AC coupled, high-pass filtered at 0.3 Hz, low-pass filtered at 300 kHz, and set to a gain of ten. The resulting signal was amplified further using an oscilloscope amplifier (model 5A20N, Tektronix, Beaverton, Ore.). The output of the oscilloscope amplifier was led into an antialiasing filter (120 dB/octave, model LP-120, Unigon Industries, White Plains, N.Y.), and digitized using a 12-bit A-to-D converter (model DAS-250, Datel, Canton, Mass.). Data were acquired using a custom interface attached to a PDP-11/34A computer system (Digital Equipment Corp., Maynard, Mass.).

Two digitization bandwidths, 2.16 and 21.6 kHz, were used in order to obtain good low- and high-frequency resolution, respectively. Signal averaging in the time domain was also used to improve the effective signal-to-noise ratio (*see* Clausen & Fernandez, 1981). Five blocks in the linear range of 2 to 910 Hz were collected and averaged, and ten blocks in the linear range of 20 Hz to 9.1 kHz were collected and averaged. The total data collection time was less than 5 sec for each run. The data were merged producing 900 frequency points, which were subsequently reduced to 100 frequencies by selecting points based on a logarithmic distribution between 2 Hz and 9.1 kHz. All signal averaging and Fourier computations were performed using floating-point arithmetic (7 to 8 significant digits).

Determination of the Membrane Circuit Parameters

The impedance data were fitted by morphologically based equivalent-circuit models (*see* Results) using the method of Clausen et al. (1979). The impedance was represented by the Bode plots, which plot Log magnitude and phase angle as a function of frequency. A derivative-free Levenberg-Marquardt algorithm (Brown & Dennis, 1972) was used to minimize the sum of the squared deviations between the model-predicted impedance and the measured magnitude and phase plots (200 data points), by adjusting the circuit parameters of the equivalent-circuit model. Convergence to a minimum sum-square error was assumed when the model parameters changed by less than 0.1% during successive iterations of the procedure.

The R-factor (Hamilton, 1964) was calculated as an objective measure of the quality of each of the curve fits. The R-factor is interpreted as the average relative discrepancy between the data and the model-predicted impedance. R-ratio tests were performed to compare the quality of fits obtained by two equivalent-circuit models (*see* Results) which differ in the number of adjustable circuit parameters. The R-ratio test (a modified F-test) is used to verify that the quality of the data warrants the additional circuit parameters which invariably result in better fits by the model. In addition, after each curve fit we calculated estimates of the standard deviations of the best-fit circuit parameters. If a standard deviation exceeded 10% of the parameter value, then

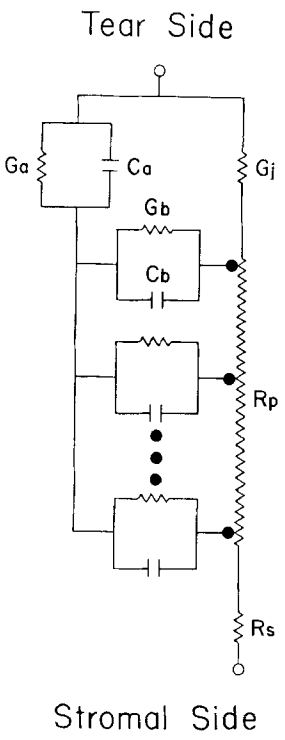

Fig. 1. Distributed equivalent-circuit model for corneal epithelium. Consult the text for descriptions of the symbols. The impedance of the corneal endothelium is not shown (*see* text)

that parameter was considered to be poorly determined by the available data and therefore was not included in subsequent analyses. It should be noted that the estimates of the parameter standard deviations are computed from a linearization of the model about the best-fit parameter set (*see* Hamilton, 1964). They do not reflect a true confidence interval for each parameter value due to the nonlinear dependence of the impedance on each parameter (*see* Valdiosera et al., 1974).

All computations were performed on the PDP-11/34A computer system. The model impedance was evaluated using double-precision (16 significant digit) arithmetic in order to obtain accurate numerical estimates of the Jacobian matrix (required by the Levenberg-Marquardt algorithm, and for the estimation of the parameter standard deviations).

Results

Equivalent Circuit Model

Clausen et al. (1979) showed that the simplest morphologically based equivalent circuit model appropriate for representing the impedance in an epithelium possessing narrow lateral spaces is the so-called distributed model shown in Fig. 1. The apical membrane is represented as a parallel resistor-capacitor (RC) circuit element where the resistor ($R_a \equiv 1/G_a$) represents the ionic conductance of the membrane, and the capacitor (C_a) represents the membrane capacitance and is proportional to membrane area. The basolateral membrane is also represented as a parallel RC circuit where the circuit elements ($R_b \equiv 1/G_b$ and C_b, respectively) have analogous interpretations. Due to the narrow width and long length of the lateral spaces, they are expected to impart a path resistance (R_p) geometrically located along the basolateral membrane from the tight junctions to the stroma. The apical membrane is a lumped impedance, but the series combination of the basolateral membrane and the lateral spaces forms a distributed impedance. The impedance of the tight junctions is considered to be purely resistive ($R_j \equiv 1/G_j$) since the cross-sectional area of the junctions is negligible compared to the other membrane areas. Finally, a small series resistance (R_s) is included to represent the finite resistance arising from the unstirred layers between the voltage-measuring electrodes and the apical and basolateral surfaces. The expression describing the transepithelial impedance is given by:

$$Z(j\omega) = \frac{Y_a + Y_b^* + G_j[Y_a Y_b^*/(Y_b/R_p) + 2(1 - \operatorname{sech}\sqrt{Y_b R_p})]}{Y_a Y_b^* + G_j(Y_a + Y_b^*)} + R_s, \quad (1)$$

where $Y_a = G_a + j\omega C_a$ is the apical membrane lumped admittance, $Y_b = G_b + j\omega C_b$ is the basolateral membrane lumped admittance, $Y_b^* = \sqrt{Y_b/R_p}\tanh\sqrt{Y_b R_p}$ is the basolateral membrane and lateral space distributed admittance, $\omega = 2\pi f$ (f in Hz) is the angular frequency, and $j = \sqrt{-1}$. For the complete derivation of Eq. (1), consult Clausen et al. (1979).[1]

Clausen et al. (1979) showed that from transepithelial impedance measurements alone, it is impossible to determine uniquely all of the above parameters, since a simpler model can be constructed where G_j mathematically lumps into the other membranes parameters. However, Clausen and Wills (1981) showed that if one obtains additional independent measurements of the apparent membrane resistance ratio, then by fitting the model subject to the constraint imposed by the measured ratio, all the model parameters can be determined uniquely. The apparent membrane resistance ratio is that which is measured using a microelectrode, but it is *not* equal to the ratio of the resistances of the apical and basolateral membranes. This ratio includes ef-

[1] There are subtle differences between our distributed model (Fig. 1) and that derived by Clausen et al. (1979) (their Fig. 1*c*). Note also that their Eq. (12) contains a typographical error. A term in the denominator of the first large term reads $(1 + Y_b G_j/T)\tanh S$, and should be corrected to read $(T + Y_b G_j/T)\tanh S$.

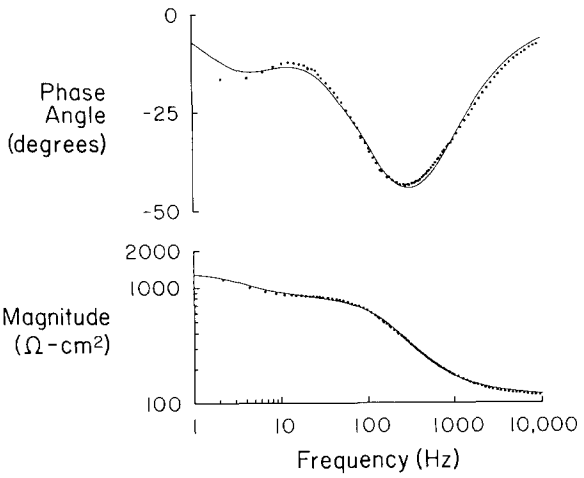

Fig. 2. Measured impedance (symbols) fitted by the distributed model (solid lines) ignoring effects caused by the small series impedance of the corneal endothelium. The deviations between the model-predicted and measured impedance are clearly seen in the phase angle plots (upper panel), but are not observable in the magnitude plots (lower panel). The data are from run 4.2 (*see* Table 1). The best-fit parameter values were: G_a 1.6 mS/cm², C_a 2.4 μF/cm², G_b 1.2 mS/cm², C_b 79 μF/cm², R_s 110 Ωcm², R_p 430 Ωcm², G_j 0.35 mS/cm². The R-factor was 2.0%

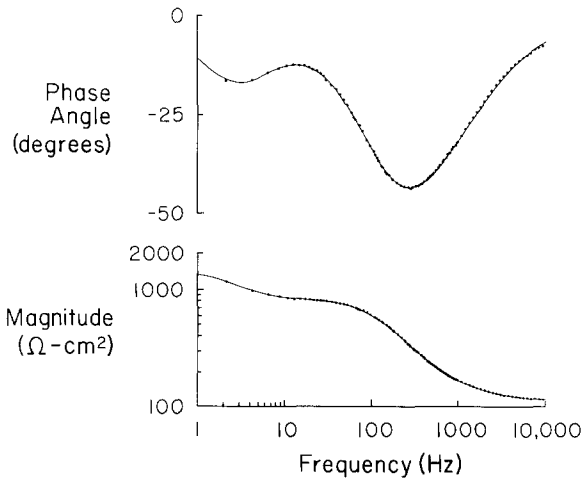

Fig. 3. Measured impedance (symbols) fitted by the distributed model (solid lines) which was modified to include the small series impedance of the corneal endothelium. The data are from run 4.2 (*see* Table 1). The deviations between the model-predicted and measured impedance seen in Fig. 2 are almost totally eliminated. The best-fit parameter values can be found in Table 2 and the text

fects caused by the unstirred layer resistances on either side of the tissue (we assume that half of R_s appears on each side), as well as the distributed lateral space resistance, and is given by:

$$\alpha = (R_a + R_s/2)/(\sqrt{R_p R_b}\coth\sqrt{R_p/R_b} + R_s/2). \quad (2)$$

In all curve fits, α was specified and held constant at its measured value, and either R_a or R_b was calculated from Eq. (2) involving α and the other parameters.

Figure 2 shows a curve fit of the distributed model (lines) to a representative data set (symbols). In all cases, the model was incapable of describing the data accurately, the deviations being more apparent in the phase-angle plot (upper panel) than in the magnitude plot (lower panel). This inadequacy of the distributed model prompted us to reevaluate simplifying assumptions inherent to the model.

The most plausible explanation for the inability of the distributed model to fit the data arises from other cell layers uncoupled electrically from the epithelial layer. One such layer which is still present in our preparation is the corneal endothelium, whose impedance properties have been measured in the rabbit (Lim & Fischbarg, 1981). These investigators found that their data could be adequately described by an equivalent circuit composed of a resistor (R_x) equal to 20 to 75 Ωcm², in parallel with a capacitor (C_x) equal to 0.6 μF/cm². Although this impedance (in series with the corneal epithelium) is a small fraction of the transepithelial impedance, it is expected to cause small phase angle deviations (*ca.* 2 degrees) at high frequencies. Attempts to fit the distributed model to the high-frequency data could therefore result in even larger deviations in the lower-frequency domain, like those observed in Fig. 2, where the number of data points is less numerous.

The distributed model was therefore modified to include corrections for the finite endothelial impedance by adding the *RC* circuit describing the endothelial impedance, and by allowing the fitting procedure to determine these circuit values. This resulted in a large and significant improvement in all of the fits ($P \ll 10^{-6}$, as determined by R-ratio tests). Figure 3 shows the data in Fig. 2 fitted by the modified model. In this particular set of data, R_x and C_x were 21 Ωcm² and 6.5 μF/cm², respectively, and the residual fit error (R-factor) decreased from 2.0% (Fig. 2) to 0.45% (Fig. 3). The average estimates for R_x and C_x (seven tissues) were 19 ± 2 Ωcm² and 5.1 ± 0.8 μF/cm² (SEM, n = 19), respectively. The mean R-factor was 0.59 ± 0.04%, and never exceeded 1%.

Membrane Parameters

We report results obtained from seven different preparations, comprising 19 different experimental states using epinephrine and furosemide to alter the rate of Cl^- secretion. Recall that in each prepara-

Table 1. DC parameters[a]

Run	State	I_{sc} (μA/cm^2)	V_t (mV)	α	V_b (mV)
1.1	Control	35	−42	0.55	−83
1.2	Epinephrine	43	−42	0.50	−81
1.3	Epinephrine	39	−41	0.61	−81
2.1	Control	31	−41	0.50	−78
2.2	Control	26	−39	0.69	−77
2.3	Epinephrine	31	−35	0.42	−74
2.4	Furosemide	12	−21	1.26	−79
3.1	Control	20	−28	1.09	−84
3.2	Epinephrine	26	−31	1.03	−87
3.3	Furosemide	13	−17	1.14	−80
4.1	Control	51	−44	0.32	−89
4.2	Furosemide	22	−31	0.69	−84
4.3	Furosemide	18	−29	1.10	−96
5.1	Control	38	−34	0.61	−86
5.2	Furosemide	20	−22	0.71	−88
6.1	Control	11	−28	1.63	−99
6.2	Epinephrine	12	−28	0.93	−72
7.1	Control	33	−35	0.50	−83
7.2	Furosemide	9.8	−18	0.68	−75

[a] Experimental state of each tissue (*see* Materials and Methods), short-circuit current (I_{sc}), transepithelial voltage (V_t), mean open-circuit basolateral membrane voltage (V_b), and the mean membrane resistance ratio (α), for each impedance run (*see* Table 2). Voltages are measured with respect to the stromal side. The numbers in the first column identify the tissue and the corresponding impedance run (e.g., 4.2 is the second impedance run for tissue 4).

tion, Cl^- transport was increased by the addition of 0.1 mM epinephrine to the stromal bathing solution, and/or was decreased by washing and by the addition of 1 mM furosemide. The DC electrical properties of each of the tissues are summarized in Table 1, which shows short-circuit current, transepithelial voltage (V_t), and mean values for the membrane resistance ratio and basolateral membrane voltage (V_b) determined using microelectrodes. The best-fit parameter estimates for each of the impedance runs are shown in Table 2. Each row in Table 2 is identified by a run number corresponding to the experimental conditions shown in Table 1.

Membrane Areas

Since nearly all biological membranes exhibit a specific capacitance of approximately 1.0 μF/cm^2 (Cole, 1972; Clausen et al., 1979), we can use the different membrane capacitance values as estimates of the membrane areas. The mean value for C_a is 2.6 μF/cm^2 (Table 3), implying that the apical membrane is slightly folded and exhibits an area approximately 2.6 times the nominal chamber area. The mean basolateral membrane capacitance is 94 μF/cm^2 (Table 3), which implies that the basolateral membrane area exceeds the apical membrane area by a factor of 94/2.6 = 36.

Table 2. Membrane parameters determined from the impedance analysis[a]

Run	State	G_a (mS/cm^2)	C_a (μF/cm^2)	G_b (mS/cm^2)	C_b (μF/cm^2)	R_p (Ωcm^2)	R_s (Ωcm^2)	G_j (mS/cm^2)	R-factor (%)
1.1	Control	1.4	2.9	0.82	86	320	130	0.54	0.68
1.2	Epinephrine	2.3	2.6	1.2	89	210	140	0.56	0.58
1.3	Epinephrine	2.2	2.7	1.4	100	230	140	0.39	0.66
2.1	Control	2.0	2.3	1.0	89	230	110	0.31	0.57
2.2	Control	1.4	2.3	1.1	93	290	110	0.26	0.57
2.3	Epinephrine	2.4	2.3	0.99	82	190	110	0.41	0.40
2.4	Furosemide	1.0	2.2	1.6	120	410	110	0.06*	0.55
3.1	Control	0.56	3.0	0.67	61	440	130	0.73	0.31
3.2	Epinephrine	1.1	2.7	1.2	97	280	130	0.48	0.42
3.3	Furosemide	0.90	2.5	1.1	120	270	130	0.40	0.42
4.1	Control	3.4	2.4	1.0	79	170	110	0.63	0.71
4.2	Furosemide	1.6	2.5	1.2	100	290	110	0.18	0.45
4.3	Furosemide	0.98	2.4	1.3	110	370	110	0.18	0.45
5.1	Control	2.2	3.2	1.4	110	420	110	0.62	0.74
5.2	Furosemide	1.1	3.0	0.85	100	310	110	0.53	0.49
6.1	Control	0.78	2.7	1.6	100	480	100	0.00*	0.83
6.2	Eprinephrine	0.98	2.5	1.1	97	600	99	0.00*	0.55
7.1	Control	2.7	2.2	1.4	94	230	90	0.26	1.0
7.2	Furosemide	0.74	2.4	0.55	59	570	88	0.46	0.80

[a] Best-fit membrane parameters obtained by fitting the impedance by the distributed model. Consult the text for description of the symbols. The run number (first column) corresponds to the tissue and experimental condition shown in Table 1. (*) G_j could not be distinguished statistically from zero, as reflected by a negligible value and a large parameter standard deviation (*see* Materials and Methods).

In a tissue having a convoluted surface, the amount of membrane present will always exceed the nominal chamber area. Hence, C_a is more appropriate than chamber area for normalizing the electrical parameters to tissue area (Lewis & Diamond, 1976; Clausen et al., 1979). Similarly, the specific ionic conductance of the basolateral membrane can be estimated by normalizing G_b to C_b as an estimate of the actual area of folded basolateral membrane present. It should be emphasized that due to the large basolateral capacitance, the specific conductance of this membrane is much less than that calculated using chamber area as a normalization factor. Area-normalized values for the junctional conductance and the lateral space resistance, as well as the specific conductance of the basolateral membrane, are shown in Table 3.

Apical Membrane Conductance

Using the apical membrane capacitance as a measure of the epithelial surface area, we can normalize the apical membrane conductance G_a and short-circuit current I_{sc}, resulting in values with units mS/μF and μA/μF, respectively. A plot of these normalized values with respect to one another results in the linear relationship shown in Fig. 4. The intercept is not significantly different from zero which shows that the apical membrane possesses no measurable leak conductance (a conductance unrelated to the Cl^- transport rate). The linearity of the G_a versus I_{sc} relationship implies that over the range of different transport rates (4.0 to 21 μA/μF), the net transport of Cl^- is modulated primarily by changes in the conductance of the apical membrane and not by changes in the net driving force for Cl^- exit.

I_{sc} essentially represents the transepithelial Cl^- transport rate under short-circuit conditions (Zadunaisky, 1966), but it does not equal the transcellular Cl^- current under open-circuit conditions (I_{cell}). I_{cell} will be equal and opposite to the paracellular current through the tight junctions and lateral spaces. Given the values for G_j and R_p (Table 2), and V_t (Table 1), I_{cell} can be calculated using the following relationship: $I_{cell} = V_t/(1/G_j + R_p)$.

When we plot G_a versus I_{cell}, after normalizing both values to C_a, we obtain the linear relationship seen in Fig. 5. The slope of the relationship (0.10 mV^{-1}) is different from that obtained in Fig. 4 (0.063 mV^{-1}) simply reflecting the different net driving forces for apical membrane chloride exit under open- versus short-circuit conditions. The zero-current intercept is also not significantly different from zero, as was the case observed in Fig. 4.

The reciprocal of the slope in Fig. 5 (10 mV) is a measure of the net driving force for apical membrane Cl^- exit under open-circuit conditions. Since it is known that the apical membrane is essentially Cl^- permselective (Reuss et al., 1983), and possesses no appreciable leak conductance (confirmed by the zero intercept in Figs. 4 and 5), I_{cell} is equal to the product of the Cl^- electrochemical driving force and the apical membrane conductance:

Table 3. Average circuit parameters[a]

	Mean	SEM
Values Normalized to Epithelial Area		
C_a (μF/cm^2)	2.6	0.065
C_b (μF/cm^2)	94	3.7
G_b (mS/cm^2)	1.1	0.065
G_j (mS/cm^2)	0.43	0.041
R_p (Ωcm^2)	331	29
R_s (Ωcm^2)	114	3.3
Values Normalized to Membrane Capacitances		
G_j (mS/μF) (normalized to C_a)	0.17	0.013
R_p ($\Omega\mu$F) (normalized to C_a)	858	81
G_b (μS/μF) (normalized to C_b)	12	0.43

[a] Mean values of the epithelial circuit parameters that were found to be independent of the rate of active Cl^- transport (*see* text). The individual parameter estimates are found in Table 2. The mean values and standard errors are from 19 impedance runs, except for G_j which is the average from 16 runs (values for runs 2.4, 6.1 and 6.2 were not averaged, *see* legend to Table 2).

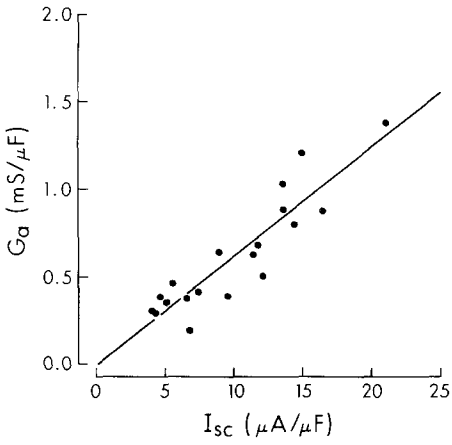

Fig. 4. Relationship between apical membrane conductance (G_a) and the short-circuit current (I_{sc}) measured 500 msec after clamping the transepithelial voltage (V_t) to zero. Both values are normalized by the apical membrane capacitance (C_a) as a measure of the area of tissue present in the chamber. The values for G_a can be found in Table 2, and the corresponding values for I_{sc} can be found in Table 1. The slope of the regression line is 0.063 ± 0.007 mV^{-1} and is highly significant ($P < 2 \times 10^{-7}$), as determined by an F-test. The intercept is −0.013 ± 0.079 mS/μF and is not significantly different from zero. The correlation coefficient (r) was 0.91

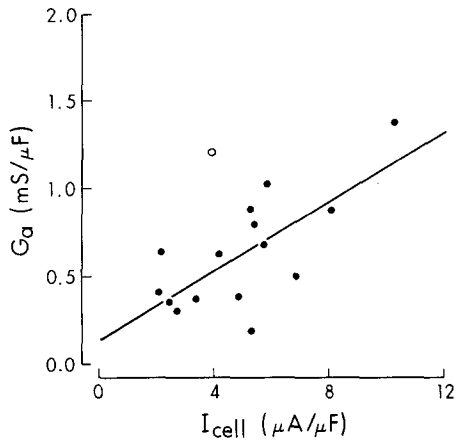

Fig. 5. Relationship between the G_a and the open-circuit transcellular current (I_{cell}), both normalized by C_a. I_{cell} is equal to the product of V_t (Table 1) and the paracellular conductance (the series combination of G_j and R_p, Table 2); it could not be determined in three cases (runs 2.4, 6.1 and 6.2, *see* Table 2). The slope of the regression line equals 0.10 ± 0.03 mV^{-1} and is statistically significant ($P < 0.003$). The intercept equals 0.13 ± 0.15 mS/μF and is not significantly different from zero. The correlation coefficient equals 0.71. The open circle was not included in the regression since its standardized residual was equal to 2.3 (*see* Ryan et al., 1976)

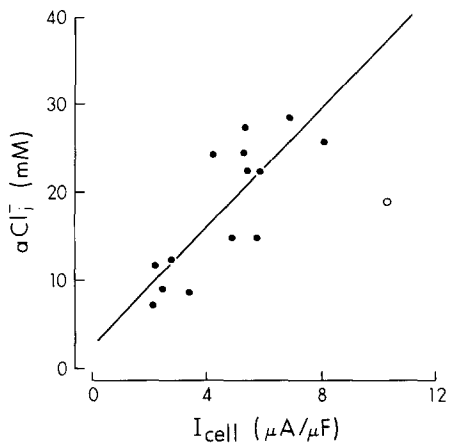

Fig. 6. Relationship between the calculated intracellular Cl^- activity (aCl_i^-) and I_{cell}. The slope of the regression line equals 3.4 ± 0.7 mM/(μA/μF) and is highly significant ($P < 0.0004$). The intercept is 2.7 ± 3.4 mM. The correlation coefficient equals 0.81. The open circle was not included in the regression analysis since its standardized residual was equal to 2.3

$$I_{cell} = G_a(V_a - E_{Cl}). \quad (3)$$

Since we have measurements of the apical membrane voltage ($V_a = V_t - V_b$, *see* Table 1), and since we know the tear Cl^- activity (85 mM, assuming a Cl^- activity coefficient of 0.75), we can obtain an estimate of the intracellular Cl^- activity (aCl_i^-) from the Nernst equation. Our mean value for E_{Cl} is 41 ± 3 mV ($n = 15$) and the mean value for aCl_i^- is 18 ± 2 mM. We also find that aCl_i^- increases with transport rate, and this is shown in Fig. 6.

Basolateral Membrane Conductance

The specific conductance of the basolateral membrane (12 μS/μF, *see* Table 3) was found not to vary with transport rate. Since G_b is predominantly a K^+ conductance (Reinach & Nagel, 1985), and since Cl^- secretion is coupled to a basolateral membrane K^+ influx (via the Na/2Cl/K symport and the Na,K-ATPase), this result implies that increasing the rate of transport is coupled with increases in the net driving force for basolateral K^+ exit. We should also note that the electrochemical gradient across the basolateral membrane is expected to vary with distance along the lateral spaces. A voltage gradient will be established along the length of the lateral spaces resulting from paracellular current flow across the lateral-space resistance. This gradient equals the product of I_{cell} and R_p and has a mean value of −3.7 ± 0.5 mV ($n = 16$), measured from the tight junctions to the stromal solution.

The predicted increase with transport of the net driving force for K^+ exit may be due to an increase in the K^+ chemical gradient across the basolateral membrane resulting from an increase in the intracellular K^+ activity (aK_i^+). We can compute the net driving force for K^+ exit under steady-state open-circuit conditions if we make the following assumptions: (1) the small lateral-space voltage gradient is negligible compared to the gradients across the basolateral membrane; (2) the Na/2Cl/K symport is nonconductive (Thurman & Reinach, 1986); (3) the Na,K-ATPase is also nonconductive and possesses a 3 Na^+ to 2 K^+ stoichiometry; and (4) G_b is essentially permselective for K^+ (Reinach & Nagel, 1985). Under these conditions, the basolateral membrane Cl^- entry rate through the symport equals I_{cell}, and is coupled with Na^+ and K^+ entry rates equal to $I_{cell}/2$. The Na,K-ATPase will result in an outward Na^+ current equal to $I_{cell}/2$, and an inward K^+ current of $I_{cell}/3$. Accordingly, the total K^+ influx equals 5/6 I_{cell}. Finally, the K^+ efflux across the basolateral will be equal to the product of G_b and the net driving force for K^+ exit, namely

$$\frac{5}{6} I_{cell} = G_b(V_b - E_K). \quad (4)$$

Using the values of I_{cell} computed above, coupled with values for G_b (Table 2) and V_b (Table 1),

we find that the mean driving force for basolateral membrane K^+ exit equals 10.5 ± 1.4 mV (n = 16), and the mean value for E_K is −93 ± 2 mV. Finally, if we assume that the K^+ activity of the solution bathing the basolateral membrane equals that of the stromal bathing solution (1.9 mM, assuming an activity coefficient of 0.75), we can compute aK_i^+ from the Nernst equation. Its mean value is 83 ± 7 mM, but as expected, we find that aK_i^+ increases with increasing transport rate (Fig. 7).

Parameters that are Independent of Transport Rate

The best-fit circuit parameters were plotted against I_{cell} (which ranged from 5 to 25 $\mu A/cm^2$) and for each parameter, a regression analysis was performed. No correlation was found between I_{cell} and the following parameters, as indicated by an insignificant correlation coefficient and slope (F-test): C_a, C_b, G_b, G_j, R_p and R_s. Their mean values are reported in Table 3. Recall that R_s is the sum of the resistances of the unstirred layers, and the resistance of the stroma. In the absence of the epithelium, the resistance between the transepithelial voltage electrodes was 105 Ωcm^2, implying that the stromal resistance equals 114 − 105 = 9 Ωcm^2 (*see* Table 3).

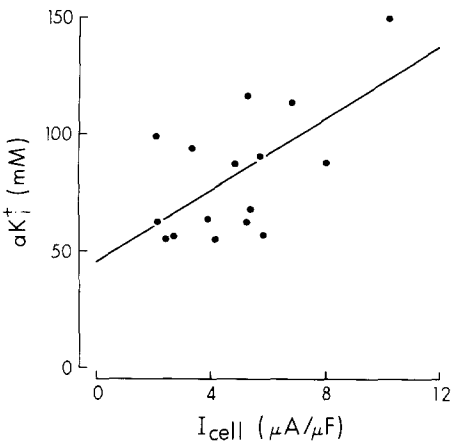

Fig. 7. Apparent relationship between the calculated intracellular K^+ activity (aK_i^+) and I_{cell}. The slope of the regression line equals 7.7 ± 2.6 mM/($\mu A/\mu F$) and is statistically significant (P = 0.01). The intercept equals 45 ± 14 mM. The correlation coefficient equals 0.62. It should be noted that the calculation of aK_i^+ ignores possible effects resulting from the Na^+ conductance of the basolateral membrane and decreases in the K^+ activity of the stromal unstirred layers. These effects would tend to increase the intercept and reduce the apparent slope (*see* text)

Discussion

Impedance analysis techniques, combined with DC measurements of the transepithelial and intracellular electrical parameters, were used to investigate the mechanism of active Cl^- transport across the frog corneal epithelium. The major reasons for undertaking this study were: (1) to utilize an independent method to measure the different membrane ionic conductances, (2) to obtain estimates of the membrane areas thereby permitting the calculation of the specific conductances of the different membranes, (3) to investigate the degree of coupling between the different cell layers, and (4) to investigate how changes in the rate of active Cl^- transport might be mediated by changes in the membrane parameters.

DC circuit analysis techniques require the use of agents that alter the rate of active Cl^- transport in order to determine apical, basolateral, and paracellular conductances, from measurements of transepithelial conductance and membrane resistance ratios. In our studies, such agents were used solely to vary the transport rate over a wide range of values. We did not have to make any assumptions about the selectivity of action of any of these agents, as was requisite in the earlier studies. Nevertheless, the impedance methods result in parameter estimates that are comparable with results from these previous studies (*see below*). This agreement between the two methods in satisfying since it provides mutual validation of the different methods. Notably, it provides direct experimental evidence that the assumptions regarding specificity of the transport-altering agents were indeed correct.[2]

Corneal Endothelium

A small series impedance consisting of a parallel RC circuit (R_x and C_x) had to be included with the distributed model of the epithelium in order to correct for small expected phase deviations resulting from the impedance of the corneal endothelial layer. This circuit does not analogously represent the observed morphology of the endothelium since one would expect that a more complicated circuit would be required. However, Lim and Fischbarg (1981) showed that due to the low endothelial paracellular resistance, a simple RC circuit is sufficient where R_x represents the endothelial paracellular resistance,

[2] This is not to say that these agents act solely on one membrane. For example, furosemide may inhibit an electrically silent ionic pathway on the basolateral membrane, but may subequently result in ionic conductance changes in the apical membrane.

and C_x represents the endothelial effective capacitance (the product divided by the sum of the endothelial apical and basolateral membrane capacitances). The earlier measurements of R_x and C_x were obtained from rabbit corneal endothelium, hence we have no reason *a priori* to expect agreement with our measurements. Moreover, our dissection and mounting technique certainly results in damage to the endothelium. Nevertheless, our mean value for R_x (19 Ωcm^2) compares favorably with the earlier values measured from rabbit (20 to 75 Ωcm^2) indicating that frog corneal endothelium also possesses a highly conductive paracellular pathway. However, our mean value for C_x (5.1 $\mu F/cm^2$) compares poorly with the value measured in rabbit (0.6 $\mu F/cm^2$), thereby suggesting that the endothelial membrane areas in frog are larger than in rabbit.

Apical Membrane Area

The apical membrane capacitance is significantly greater than 1 $\mu F/cm^2$, implying that the apical membrane is folded. High resolution micrographs show that the apical membrane in human (Kuwabara, 1983) and frog (S.D. Klyce, *personal communication*) corneal epithelium possesses microplicae which are expected to increase apical membrane area and are therefore consistent with this notion. Moreover, planimetry measurements of frog cornea micrographs (S.D. Klyce, *personal communication*) show that the microplicae increase the apical membrane surface area by an average factor of 3.1 (range 1.8 to 4.5). This measured amplification factor is in remarkable agreement with our mean apical capacitance of 2.6 $\mu F/cm^2$ when one assumes a specific membrane capacitance of *ca.* 1 $\mu F/cm^2$.

Cell Coupling

The frog corneal epithelium consists of between five and six distinct cell layers, but these layers have been shown to be connected by intracellular low-resistance pathways (Klyce, 1972). The distributed model tacitly assumes one effective epithelial cell layers, and its ability to fit the measured impedance exceptionally well supports this notion of electrical coupling between the layers. However, the goodness of fit alone is not a reliable indicator of cell coupling. In other multi-cell-layer epithelia where it is known that the layers are not coupled (notably rabbit urinary bladder) the distributed model is also capable of fitting the data accurately (Clausen et al., 1979). Our strongest evidence for cell coupling in corneal epithelium arises from the measured value of the basolateral membrane area, as reflected by C_b. In the planar epithelium rabbit urinary bladder, which possesses only one functional transport layer, C_b/C_a equals approximately five, and this value is supported by micrographs which show roughly cuboidal geometry where one would expect approximately five times more basolateral area than apical area. If the cell layers in corneal epithelium were coupled, then one would expect to find a five- to sixfold increase in basolateral area (compared to apical area) for each coupled cell layer. With five to six layers, one would therefore expect to measure a basolateral area, and hence C_b, that is between 25 and 36 times greater than the apical area. Our mean value for C_b is 94 $\mu F/cm^2$, which is 36 times larger than C_a, and is therefore consistent with the notion of a coupled syncytial epithelium. Finally, we should note that numerous gap junctions between the epithelial cells have been observed in human (Kuwabara, 1983) and more recently in frog (M. Hirsch, *personal communication*) cornea, which provides anatomical evidence for cell coupling in the tissue.

Basolateral and Paracellular Conductances

Our mean value for G_b was 1.1 mS/cm^2 and is comparable but slightly higher than the value previously reported (0.45 to 0.93 mS/cm^2, *see* Nagel & Reinach, 1980; Reuss et al., 1983). We find no evidence for an increase in G_b with transport rate, as was reported by Nagel and Reinach (1980). Membrane resistance ratios are near unity in corneal epithelium (*see* Table 1), suggesting that G_b is comparable to G_a. However, this should not be interpreted as suggesting that the two membranes' specific conductances are comparable. Using C_b to normalize G_b to unit area of membrane, we find that the specific conductance of the basolateral membrane is exceedingly low at 12 $\mu S/\mu F$ (specific resistance of 84 $k\Omega\mu F$), indicating that this membrane is nearly impermeable to ions [the putative neutral Na/2Cl/K symport process though to exist within this membrane appears to be electrically silent (Thurman & Reinach, 1986) and therefore does not contribute to the membrane's conductance]. The physiological significance of this low basolateral membrane conductance remains to be investigated, but it is tempting to speculate that it results in little ionic recirculation between the cell interior and the stromal bath. This would minimize metabolic energy expenditure for the maintenance of cell volume and ionic composition, which would be advanta-

geous for the cornea since it is not in close contact with capillaries. Conservation of energy might be essential since a large number of intracellular organelles (e.g., mitochondria) would be expected to scatter light and render the tissue opaque (Mathias et al., 1979).

Earlier studies report a paracellular (shunt) conductance ranging from 0.13 to 0.24 mS/cm^2 (Nagel & Reinach, 1980; Reuss et al., 1983), whereas we find a junctional conductance G_j equal to 0.43 mS/cm^2, indicating that the epithelium is approximately twofold more leaky than was previously thought. Recall, however, that the paracellular conductance is composed of the series combination of G_j and R_p. We compute a mean paracellular conductance of 0.38 ± 0.03 mS/cm^2, which is comparable but still higher than the earlier reports.

Apical Membrane Conductance

The relationships between G_a and I_{sc} (Fig. 4) and G_a and I_{cell} (Fig. 5) show that there is no measurable apical membrane leak conductance, and that the transport rate is dependent primarily on the apical membrane conductance. Since it is known that I_{sc} is nearly accounted for by active Cl^- transport, these results support the notion that the apical membrane is essentially Cl^- permselective. This finding is in agreement with that of Reuss et al. (1983) who obtained this same result using DC methods involving ionic bathing solution substitutions and measurements of intracellular ionic activities. However, these authors also observed a small but finite apical membrane conductance to K^+. Since our data indicate that there is no measurable apical membrane leak conductance, this suggests that the K^+ conductive pathway is common to that of Cl^-. Cl^- channels possessing a finite K^+ permeability have been observed in other epithelia [notably in the basolateral membrane of rabbit urinary bladder (Hanrahan et al., 1985)], which further supports this notion.

Apical Membrane Cl^- Exit

The linearity of the G_a versus I_{sc} relationship (Fig. 4) implies that the net driving force for apical membrane Cl^- exit remains essentially constant and independent of the rate of transport. The reciprocal slope of this relationship (16 mV) is a measure of the driving force. However, this calculated net driving force is predicted for the nonphysiological condition where the epithelium is momentarily switched from open- to short-circuit conditions. Moreover, it requires the assumption that the apical membrane current-voltage relationship is linear since the membrane conductance was determined from open-circuit impedance measurements.

Under open-circuit conditions, the Cl^- transport rate is represented by I_{cell}, which was determined from measurements of V_t and the paracellular conductance. G_a and I_{cell} were also found to be correlated (Fig. 5), and this further supports the notion that the Cl^- transport rate is dependent primarily on G_a and not on changes in the net driving force for Cl^- exit. Our estimate for the net driving force is in good agreement with previously reported values determined from Cl^--selective electrode measurements by Reuss et al. (1983) and Patarca et al. (1983). These investigators measured values of 10 to 16 mV which are comparable to our calculated value of 10 mV determined from the reciprocal slope of Fig. 5. Our calculated mean value for E_{Cl} is 41 mV, and is in agreement with previously reported values ranging between 33 and 45 mV (Nagel & Reinach, 1980; Patarca et al., 1983).

We should note that transport-dependent changes in the net driving force for Cl^- exit have been measured with Cl^--selective electrodes (Patarca et al., 1983), but these changes are much smaller than the concomitant changes in G_a and are probably undetectable using our methods. Our results indicate that the epithelium maintains a balance between the electrical and chemical forces favoring Cl^- exit. As I_{cell} increases, V_a and E_{Cl} both depolarize by approximately the same amount such that their difference (the net driving force) remains unchanged. Since the tear side Cl^- activity was kept constant in our experiments, this means that intracellular Cl^- activity must increase with transport, and this is shown in Fig. 6.

Basolateral Membrane K^+ Exit

Cl^- transport in corneal epithelium results in a concomitant influx of Na^+ and K^+ across the basolateral membrane owing to the putative Na/2Cl/K-symport and the Na,K-ATPase. We postulated that at steady state, the Cl^- transport results in an outward K^+ current accounting to approximately 5/6 I_{cell} via a basolateral membrane K^+-conductive pathway. Measurements of G_b and the basolateral membrane voltage allowed us to estimate the net driving force for K^+ exit, and to investigate how the driving force changes with the rate of transport.

Unlike the apical membrane conductance, G_b was *not* found to increase with I_{cell}, and this result implies that increases in the transport rate result in increases of the net driving force for K^+ exit. The simplest explanation for this is that aK_i^+ increases

with the rate of transport, owing to the increased basolateral membrane K^+ flux, and this is seen in Fig. 7. However, we are reluctant to place much significance on this apparent result since at least two of the assumptions inherent to the computation of aK_i^+ may not be correct.

In computing aK_i^+, we assumed that G_b was entirely K^+ selective, but in reality, a small but finite basolateral membrane Na^+ conductance has been reported (Reinach & Nagel, 1985). This Na^+ conductance would be expected to result in an inward Na^+ current which would indirectly cause an additional inward K^+ current due to stimulation of the Na,K-ATPase. Since this was ignored, the calculated values of aK_i^+ are probably underestimates of the true values, especially at low transport rates.

Another assumption inherent to the computation of aK_i^+ was that the lateral-space K^+ activity equaled the stromal solution bulk activity. Due to the large relative intracellular volume compared to the volume of the lateral spaces, and due to an undoubtedly substantial stromal unstirred layer, one might expect that Cl^- transport could cause a significant decrease in the K^+ activity of the extracellular solution adjacent to the basolateral membrane. This would produce an increased K^+ chemical gradient and hence an increased driving force for K^+ exit, but would not necessarily result in a significant increase in aK_i^+ owing to the small volume of the lateral spaces compared to the intracellular volume. Note that this effect would be expected to be most prominant at high transport rates, and would result in calculated values of aK_i^+ that are overestimates of the true values.

Summary

We summarize our major results and conclusion as follows:

1. The measured impedance from frog corneal epithelium can be analyzed quantitatively using a simple morphologically based equivalent-circuit model. When coupled with DC measurements of apparent membrane resistance ratios, the analysis of the impedance allows one to determine all the membrane circuit parameters without using agents that alter the rate of active Cl^- transport, as is required with DC techniques. The results obtained agree well with those obtained earlier, thereby providing mutual validation of the different methods.

2. Our data are consistent with the notion that the different cell layers of the epithelium are electrically coupled via low-resistance junctions, thereby allowing the different layers to function together as a syncytium.

3. Although the apical and basolateral membrane conductances are comparable, the specific ionic conductance of the basolateral membrane is very low indicating that it imposes a significant barrier to passive ion flow.

4. Since the apical membrane possesses no measurable leak conductance, a reported apical membrane K^+ conductance probably shares the Cl^- conductance pathway.

5. The rate of Cl^- transport is modulated mainly by changes in the conductance of the Cl^--selective apical membrane. Our calculations suggest that intracellular Cl^- activity increases with transport thereby maintaining a nearly constant net driving force for apical membrane Cl^- exit.

6. Since the basolateral membrane conductance does not vary with the rate of transport, we find that the net driving force for basolateral membrane K^+ exit increases with transport, possibly resulting from an increase in intracellular K^+ activity.

We thank Dr. S.D. Kylce for kindly providing us with planimetry measurements detailing the degree of apical membrane infolding, and for helpful discussions. We also thank Dr. M. Hirsch for performing freeze-fracture electronmicroscopy which confirmed the existence of gap junctions in our tissue. Finally, we thank Drs. S.A. Lewis and N.K. Wills for many helpful discussions while this study was in progress, and for useful comments on the manuscript. This work was supported by NIH grants AM28074, EY04795, and NS19490.

References

Brown, K.M., Dennis, J.E. 1972. Derivative free analogues of the Levenberg-Marquardt and Gauss algorithms for nonlinear least squares approximation. *Numer. Math.* **18**:289–297

Clausen, C., Fernandez, J.M. 1981. A low-cost method for rapid transfer function measurements with direct application to biological impedance analysis. *Pfluegers Arch.* **390**:290–295

Clausen, C., Lewis, S.A., Diamond, J.M. 1979. Impedance analysis of a tight epithelium using a distributed resistance model. *Biophys. J.* **26**:291–318

Clausen, C., Wills, N. 1981. Impedance analysis in epithelia. *In:* Ion Transport by Epithelia. S.G. Schultz, editor. pp. 79–92. Raven, New York

Cole, K.S. 1972. Membranes Ions and Impulses. pp. 12–59. University of California Press, Berkeley, California

Greger, R., Schlatter, E. 1983. Cellular mechanism of the action of loop diuretics on the thick ascending limb of Henle's loop. *Klin. Wochenschr.* **61**:1019–1027

Greger, R., Schlatter, E. 1984. Mechanism of NaCl secretion in the rectal gland of spiny dogfish (*Squalus acanthias*). II. Effects of inhibitors. *Pfluegers Arch.* **402**:364–375

Hamilton, W.C. 1964. Statistics in Physical Science. Ronald Press, New York

Hanrahan, J.W., Alles, W.P., Lewis, S.A. 1985. Single anion-selective channels in basolateral membrane of a mammalian tight epithelium. *Proc. Natl. Acad. Sci. USA* **82**:7791–7795

Klyce, S.D. 1972. Electrical profiles in the corneal epithelium. *J. Physiol. (London)* **226:**407–429

Kuwabara, T. 1983. The eye. *In:* Histology. L. Weiss, editor. pp 1135–1176. Elsevier Biomedical, New York

Lewis, S.A., Diamond, J.M. 1976. Na transport by rabbit urinary bladder, a tight epithelium. *J. Membrane Biol.* **28:**1–35

Lewis, S.A., Eaton, D.C., Clausen, C., Diamond, J.M. 1977. Nystatin as a probe for investigating the electrical properties of a tight epithelium. *J. Gen. Physiol.* **70:**427–440

Lim, J.J., Fischbarg, J. 1981. Electrical properties of rabbit corneal endothelium as determined from impedance measurements. *Biophys. J.* **36:**677–695

Mathias, R.T., Rae, J.L., Eisenberg, R.S. 1979. Electrical properties of structural components of the crystalline lens. *Biophys. J.* **25:**181–201

Nagel, W., Reinach, P. 1980. Mechanism of stimulation by epinephrine of active transepithelial Cl transport in isolated frog cornea. *J. Membrane Biol.* **56:**73–79

Patarca, R., Candia, O.A., Reinach, P.S. 1983. Mode of inhibition of active Cl transport in the frog cornea by furosemide. *Am. J. Physiol.* **245:**F660–F669

Reinach, P., Nagel, W. 1985. Implications of an anomalous intracellular electrical response in bullfrog corneal epithelium. *J. Membrane Biol.* **87:**201–209

Reuss, L., Finn, A.L. 1974. Passive electrical properties of toad urinary bladder. *J. Gen. Physiol.* **64:**1–25

Reuss, L., Reinach, P., Weinman, S., Grady, T.P. 1983. Intracellular ion activities and Cl transport mechanisms in bullfrog corneal epithelium. *Am. J. Physiol.* **244:**C336–C347

Ryan, T.A., Joiner, B.L., Ryan, B.F. 1976. Minitab Student Handbook. p. 179. Duxbury, Boston, Massachusettes

Smith, P.L., Frizzell, R.A. 1984. Chloride secretion by canine tracheal epithelium: IV. Basolateral membrane K permeability parallels secretion rate. *J. Membrane Biol.* **77:**187–199

Thurman, C., Reinach, P. 1986. Basolateral membrane characteristics of bullfrog corneal epithelia. *Fed. Proc.* **45:**747

Valdiosera, R., Clausen, C., Eisenberg, R.S., 1974. Circuit models of the passive electrical properties of frog skeletal muscle fibers. *J. Gen. Physiol.* **63:**432–459

Welsh, M.J., Smith, P.L., Frizzell, R.A. 1983. Chloride secretion by canine tracheal epithelium: III. Membrane resistances and electromotive forces. *J. Membrane Biol.* **71:**209–218

Zadunaisky, J.A. 1966. Active transport of chloride in frog cornea. *Am. J. Physiol.* **211:**506–512

Received 25 June 1985; revised 9 January 1986